

## Research Articles



## Electrocatalysis

How to cite: *Angew. Chem. Int. Ed.* **2021**, *60*, 1909–1915 International Edition: doi.org/10.1002/anie.202011956 German Edition: doi.org/10.1002/ange.202011956

# Controlling the Surface Oxidation of Cu Nanowires Improves Their Catalytic Selectivity and Stability toward $C_{2+}$ Products in $CO_2$ Reduction

Zhiheng Lyu<sup>+</sup>, Shangqian Zhu<sup>+</sup>, Minghao Xie, Yu Zhang, Zitao Chen, Ruhui Chen, Mengkun Tian, Miaofang Chi, Minhua Shao,\* and Younan Xia\*

Abstract: Copper nanostructures are promising catalysts for the electrochemical reduction of CO<sub>2</sub> because of their unique ability to produce a large proportion of multi-carbon products. Despite great progress, the selectivity and stability of such catalysts still need to be substantially improved. Here, we demonstrate that controlling the surface oxidation of Cu nanowires (CuNWs) can greatly improve their  $C_{2+}$  selectivity and stability. Specifically, we achieve a faradaic efficiency as high as 57.7 and 52.0% for ethylene when the CuNWs are oxidized by the  $O_2$  from air and aqueous  $H_2O_2$ , respectively, and both of them show hydrogen selectivity below 12%. The high yields of  $C_{2+}$  products can be mainly attributed to the increase in surface roughness and the generation of defects and cavities during the electrochemical reduction of the oxide layer. Our results also indicate that the formation of a relatively thick, smooth oxide sheath can improve the catalytic stability by mitigating the fragmentation issue.

#### Introduction

The large amount of CO<sub>2</sub> produced from transportation and industry has raised increasing concerns in recent years because of the major environmental burdens from this gas

[\*] Z. Lyu, [+] M. Xie, R. Chen, Prof. Dr. Y. Xia School of Chemistry and Biochemistry Georgia Institute of Technology Atlanta, GA 30332 (USA)

E-mail: younan.xia@bme.gatech.edu

S. Zhu,[+] Dr. Y. Zhang, Prof. Dr. M. Shao

Department of Chemical and Biological Engineering, and Hong Kong Branch of the Southern Marine Science and Engineering Guangdong Laboratory, The Hong Kong University of Science and Technology Clear Water Bay, Kowloon, Hong Kong (P. R. China)

E-mail: kemshao@ust.hk

Dr. Y. Zhang, Z. Chen, Prof. Dr. Y. Xia

The Wallace H. Coulter Department of Biomedical Engineering, Georgia Institute of Technology and Emory University Atlanta, GA 30332 (USA)

Dr. M. Tian

Institute for Electronics and Nanotechnology, Georgia Institute of Technology, Atlanta, GA 30332 (USA)

Dr. M. Chi

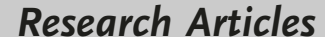
Center for Nanophase Materials Sciences, Oak Ridge National Laboratory, Oak Ridge, TN 37831 (USA)

- [+] These authors contributed equally to this work.
- Supporting information and the ORCID identification number(s) for the author(s) of this article can be found under: https://doi.org/10.1002/anie.202011956.

and the necessary increase in mitigation investment.  $^{[1,2]}$  In addition to photosynthesis, another promising route is to electrochemically convert  $CO_2$  to chemical compounds for use as fuels or feedstock. Typically, a variety of products are generated in this process, with the most common ones being CO and formate. Compared to  $C_1$  species, multi-carbon  $(C_{2+})$  products such as ethylene and ethanol are more desirable considering their higher values, larger energy densities, and broader applications. Despite the remarkable progress, it remains a grand challenge to electrocatalytically promote C-C coupling and thereby achieve high selectivity toward  $C_{2+}$  products during the  $CO_2$  reduction reaction  $(CO_2RR)$ .  $^{[1-3]}$ 

Among all the metals under consideration for CO<sub>2</sub>RR, Cu easily stands out for its ability to produce a substantial amount of oxygenates and hydrocarbons. However, for those catalysts based on pure Cu (e.g., Cu foils), they tend to suffer from a number of shortcomings, including low selectivity, poor competition with the hydrogen evolution reaction (HER), high overpotential, and compromised stability. To address these issues, the Cu nanostructures have been engineered in multiple ways, such as control of their shapes and thus surface structures, [4-7] doping with other metals or non-metals, [8-10] and complete or partial oxidation of Cu. [11-13] When switching to Cu dendrites with a rough, defective surface, for example, a faradaic efficiency (FE) as high as 57% was achieved for ethylene at a potential more negative than  $-1.4\,\mathrm{V}_{\mathrm{RHE}}$  (RHE: reversible hydrogen electrode) in 0.1 M aqueous KBr. The excellent performance was attributed to the presence of high-index facets.<sup>[5]</sup> In another study, star-shaped Cu decahedra featuring a penta-twinned structure were demonstrated with a good selectivity of 52.4% toward ethylene at  $-1.0 V_{RHE}$  in 0.1 M aqueous KHCO<sub>3</sub>. The tensile surface strain caused by the twin boundaries and the induced surface defects were proposed as a main contribution to the high C<sub>2+</sub> yields.<sup>[6]</sup>

By partially oxidizing Cu nanostructures or directly using nanostructures made of  $\text{Cu}_x\text{O}$ , improvement in catalytic performance was also achieved, including the observations of lower overpotentials and higher selectivity toward  $\text{C}_{2+}$  products. The improvement was typically ascribed to an increase in surface roughness and thus a higher density of surface defects, induced changes to the local pH, and the possible existence of residual  $\text{Cu}^{\text{I}}$  species that might serve as active sites. In one study, it was reported that when  $\text{Cu}_2\text{O}$  nanoparticles were used as catalysts, a high selectivity approaching 60% was achieved for ethylene after 6 h of electrolysis at  $-1.1\,\text{V}_{\text{RHE}}$  in 0.1 M aqueous KHCO<sub>3</sub>. The







20-nm Cu<sub>2</sub>O particles were gradually broken down into 2–4 nm particles under the negative potential, leading to an increase in the selectivity toward ethylene that finally reached 60%. The compact arrangement of small particles and the high density of grain boundaries among them were believed to be responsible for the high yield of  $C_{2+}$  products because the defective structures helped promote C–C coupling.  $^{[11]}$  In another report, plasma-activated Cu nanocubes with an oxygen content of 30% (in terms of atomic percentage) showed a higher FE toward ethylene (up to 45% at  $-1.0~V_{\rm RHE}$  in 0.1 M aqueous KHCO<sub>3</sub>) relative to those with lower oxygen contents. The key parameters were believed to be the defects induced by plasma oxidation and the surface/subsurface oxygen species, both capable of enhancing the binding of CO to the Cu surface.  $^{[13]}$ 

In an attempt to leverage the benefits arising from both shape control and surface oxidation, here we synthesize Cu nanowires (CuNWs) and then partially oxidize their surface under two different conditions to generate Cu@CuxO coresheath nanostructures. When the oxide sheath is reduced to elemental Cu, the increase in surface roughness and the penta-twinned structure intrinsic to the nanowires are able to work synergistically in promoting the generation of C<sub>2+</sub> products during CO<sub>2</sub>RR. As a result, FEs as high as 57.7 and 52.0% for ethylene are obtained at  $-1.0 V_{RHE}$  in 0.1 M aqueous KHCO<sub>3</sub> when the CuNWs oxidized by the O<sub>2</sub> from air (A-CuNWs) and aqueous H<sub>2</sub>O<sub>2</sub> (H-CuNWs) serve as catalysts, respectively. The high selectivity toward ethylene, together with C<sub>2+</sub> yields approaching 78.4 and 71.9%, is among the highest when benchmarked against all the Cubased nanostructures reported in literature (Table S1). In addition to the high selectivity, we also demonstrate that a thick and smooth oxide sheath on the CuNWs can substantially improve their catalytic stability, with H-CuNWs showing a much better stability than A-CuNWs, due to the mitigation of fragmentation and thus preservation of onedimensional (1D) morphology. This work represents the first attempt to bring a tight control to the oxidation process of CuNWs for the demonstration of its importance in determining the activity, selectivity, and stability of Cu catalysts toward CO<sub>2</sub>RR.

#### **Results and Discussion**

The preparation of a catalyst typically involved two major steps: synthesis of CuNWs in the presence of hexadecylamine and glucose, followed by surface oxidation at room temperature under different conditions. Figure S1 shows transmission electron microscopy (TEM) images of the as-prepared CuNWs with an average diameter of  $22.4 \pm 4.2$  nm and length up to several micrometers. Based on our previous report, the nanowires had a penta-twinned structure and their side surface was covered by  $\{100\}$  facets. After oxidization with the  $O_2$  from air, the 1D morphology was retained while the surface was roughened due to the formation of an oxide sheath (Figure 1 a,b). As shown in Figure 1 b, lattice fringes with a spacing of 0.21 nm, corresponding to  $\{111\}$  planes of Cu, could be observed at the central region of the nanowire,

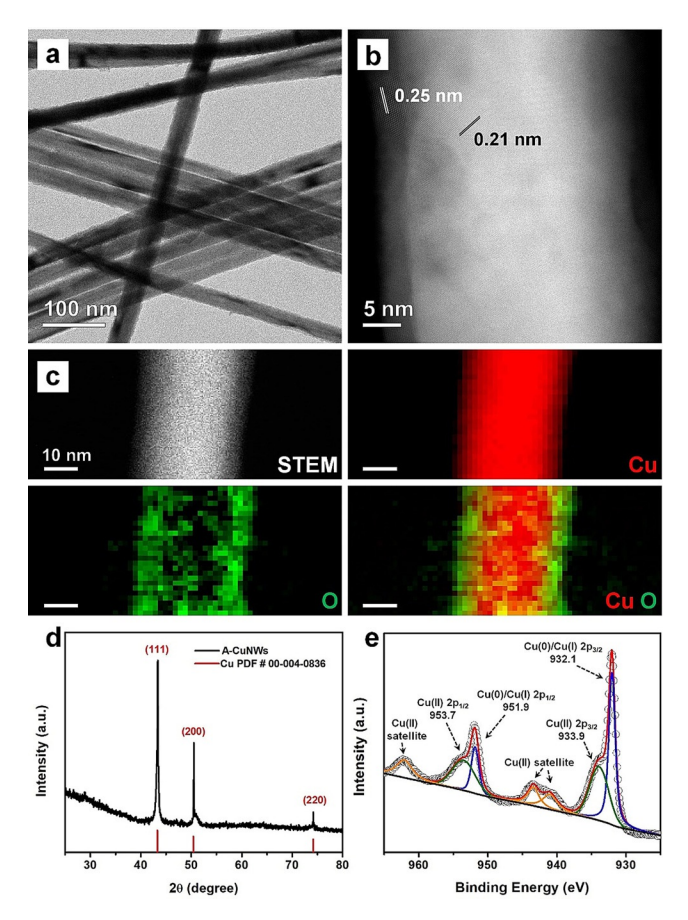


Figure 1. a) TEM and b) DF-STEM images of CuNWs covered by a thin, non-uniform sheath of  $Cu_xO$  formed through oxidation by the  $O_2$  from air (denoted A-CuNWs). c) EELS mapping, d) XRD pattern, and e) XPS spectrum recorded from the same oxidized sample.

indicating the presence of metallic Cu in the core. The fringes could hardly be observed when moving toward the surface of the nanowire, along with a decrease in contrast, suggesting the formation of oxides on the surface. At a few spots where lattice fringes could be resolved, the spacing was measured to be 0.25 nm, corresponding to the {111} planes of Cu<sub>2</sub>O. Taken together, it can be concluded that the oxide sheath was comprised of a mixture of both amorphous and crystalline copper oxides. The presence of surface oxides was also supported by the electron energy loss spectroscopy (EELS) mapping data shown in Figure 1c, where a thin layer containing oxygen could be resolved on the core made of metallic Cu. Interestingly, in the dark-field scanning transmission electron microscopy (DF-STEM) image, we observed the formation of an oxide sheath with varying thickness at different locations. Based on previous reports, it was demonstrated that the formation of copper oxides on Cu(100) facets followed an island-growth mode and it was found to be more obvious under slow oxidation kinetics.[15,16] Taken together, the non-uniform oxidation occurring on the surface of a CuNW was believed to be responsible for the formation of a Cu<sub>x</sub>O sheath with uneven thickness.

In the X-ray photoelectron spectroscopy (XPS) spectrum recorded from A-CuNWs (Figure 1e), two peaks were





resolved at 932.1 and 951.9 eV, which could be assigned to Cu<sup>0</sup> or Cu<sup>1</sup> 2p peaks. Additionally, we observed two peaks at 933.9 and 953.7 eV, together with satellite peaks around 941, 943, and 962 eV, and all of them could be assigned to Cu<sup>II</sup> 2p peaks.<sup>[17]</sup> These results indicate that the oxide sheath was made of a mix of Cu<sub>2</sub>O and CuO. In the X-ray diffraction (XRD) pattern, however, no peaks of copper oxides were observed (Figure 1 d). We only resolved three peaks at 43.4°, 50.5°, and 74.2°, corresponding to the diffraction from Cu(111), (200), and (220) planes. The absence of Cu<sub>x</sub>O peaks in the XRD pattern confirmed the dominance of amorphous phase, in agreement with our conclusion drawn from STEM imaging.

Different from the slow oxidation by the  $O_2$  from air, CuNWs covered by a relatively thicker  $Cu_xO$  sheath (H-CuNWs) were obtained when the sample was subjected to oxidation by aqueous  $H_2O_2$  (Figure 2a). The H-CuNWs had a metallic Cu core with an average diameter of  $18.5 \pm 3.4$  nm and an oxide sheath of  $6.9 \pm 0.7$  nm in thickness. As shown by the DF-STEM image in Figure 2b, both the oxide layer and the Cu core had smooth surfaces and this outcome can be attributed to the fast oxidation kinetics. Multiple nucleation sites for copper oxides were generated at the same time across

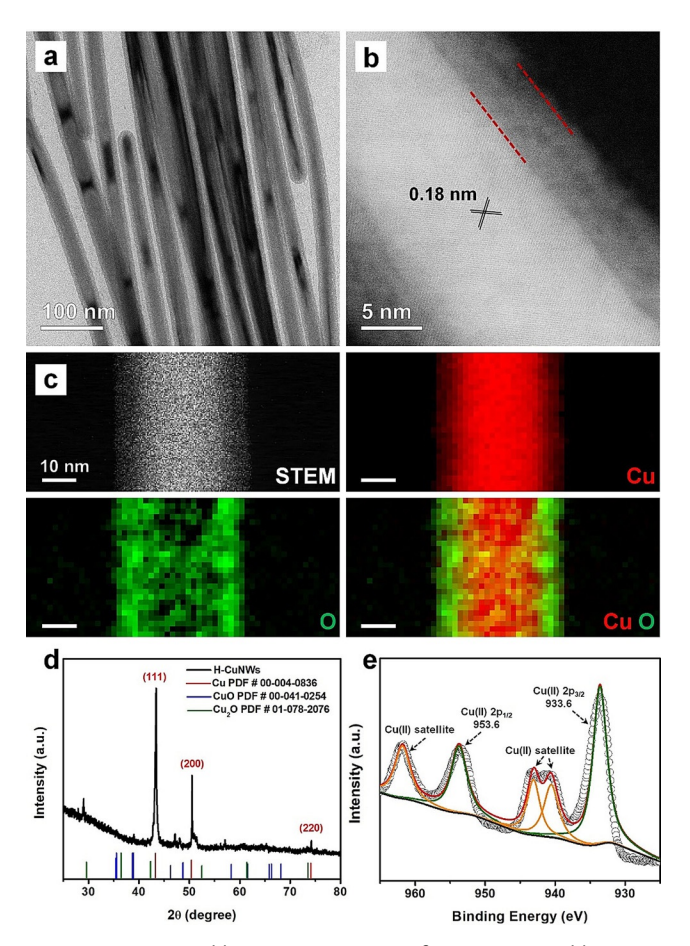
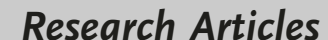


**Figure 2.** a) TEM and b) DF-STEM images of CuNWs covered by a smooth, relatively thick (ca. 6 nm) sheath of Cu<sub>x</sub>O formed through oxidation by aqueous  $H_2O_2$  (denoted H-CuNWs). c) EELS mapping, d) XRD pattern, and e) XPS spectrum recorded from the same oxidized sample.

the surface of a nanowire, leading to the formation of an oxide sheath uniform in thickness.  $^{[15]}$  The existence of  $\text{Cu}_{r}\text{O}$  layer was also verified by EELS mapping (Figure 2c). A higher intensity of oxygen was observed relative to that of A-CuNWs, consistent with the fact that H-CuNWs had a thicker layer of oxides. In the DF-STEM image, the clearly resolved lattice fringes in the core confirmed its composition as metallic Cu, while nearly no fringes were observed in the sheath. From the XRD pattern (Figure 2d), the intensity of Cu<sup>0</sup> was also the strongest, with three peaks positioned at 43.4°, 50.5°, and 74.2°. In contrast, the peaks of both Cu<sub>2</sub>O and CuO were very weak, with that at 28.9° corresponding to Cu<sub>2</sub>O and those at 39.0°, 47.0°, and 48.0° to CuO. A plausible reason for the weak intensity of copper oxides in the XRD pattern can be ascribed to the dominance of amorphous structure, which was further proven by nano-beam electron diffraction (NBED). As shown in Figure S2, rings along with irregularly distributed diffraction spots were observed in the NBED patterns recorded from selected areas of the Cu<sub>x</sub>O sheath, revealing the amorphous phase containing randomly oriented nanocrystallites. In contrast, discrete spots located at nearly the same positions could be clearly observed in the NBED patterns taken from the Cu core, with no accompanied rings, demonstrating the continuity and crystalline structure of the metallic core. [18] The composition of the surface oxides was also analyzed using XPS (Figure 2e). Different from A-CuNWs, the intensity of Cu<sup>II</sup> accounted for the vast majority and the peaks of Cu<sup>0</sup> or Cu<sup>I</sup> were barely detected, suggesting that the surface of H-CuNWs was covered by a relatively thick sheath made of CuO. In a typical process of Cu oxidation, the metallic Cu was first oxidized to Cu<sub>2</sub>O, which could be further converted to CuO in the presence of adequate oxidants. The relatively high concentration of H<sub>2</sub>O<sub>2</sub> and its fast oxidation kinetics enabled the complete oxidation of Cu, leading to the formation of a CuO-based sheath.[19,20]

In addition to microscopy evidence, the presence of oxide layer also agreed with the ultraviolet-visible (UV-vis) spectra (Figure S3). Due to the localized surface plasma resonance (LSPR) property, Cu nanostructures exhibit absorption in the visible region, and the peak position is highly sensitive to the oxidation state of Cu on the surface because of the change in dielectric constant.<sup>[21]</sup> For the freshly prepared CuNWs, A-CuNWs, and H-CuNWs, we obtained peaks located at 564, 568, and 568 nm, respectively. Compared to the as-obtained CuNWs, the peaks of both A-CuNWs and H-CuNWs were slightly red-shifted and the shift could be attributed to the surface oxidation of Cu nanostructures.<sup>[22,23]</sup>

We then compared the selectivity and activity of the CuNWs with different surface oxidation toward  $CO_2RR$  in the potential range of -0.8 to -1.2  $V_{RHE}$  in 0.1 M aqueous KHCO<sub>3</sub> (Figure 3, with details provided in the Supporting Information). Multiple products were detected, including CO, CH<sub>4</sub>, ethylene, and ethanol, and we paid special attention to the  $C_{2+}$  species, in particular, ethylene. For A-CuNWs, a FE approaching 57.7% was obtained at -1.03  $V_{RHE}$  for ethylene, together with a total efficiency reaching 78.4% for  $C_{2+}$  products. These values were among the highest selectivity for  $CO_2RR$  in a KHCO<sub>3</sub> solution, even compelling when







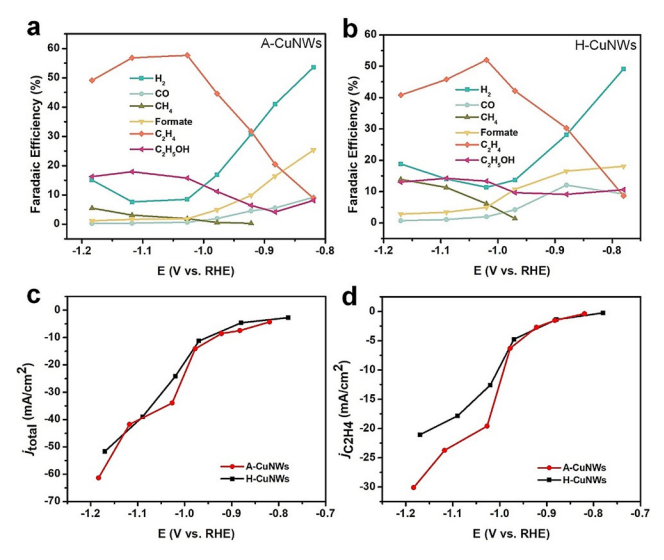


Figure 3. a,b) Faradaic efficiencies of the catalysts based on A-CuNWs and H-CuNWs, respectively. c) Total and d) partial current densities toward ethylene for the same types of catalysts in 0.1 M KHCO<sub>3</sub>. The current densities were normalized to the geometric area.

compared to the performance measured in a flow cell containing a strong alkaline electrolyte (Figure 3a and Table S1). Compared with the high yield of  $C_{2+}$  products at  $-1.03~V_{RHE}$ , the production of CO and  $CH_4$  only accounted for 0.65 and 1.9%, respectively. The FE of  $H_2$  was as low as 8.5%, indicating the effective suppression of HER. Normalized by geometric area, a total current density of 34.0 mA cm<sup>-2</sup> was achieved along with the high selectivity toward ethylene, whose partial current density reached 19.6 mA cm<sup>-2</sup> (Figure 3c,d). When normalized to the mass of catalyst, we obtained a mass activity of 384.1 mA mg<sup>-1</sup> for the selective production of ethylene (Figure S4). The high current density and mass activity of A-CuNWs demonstrate their prominent performance in electrochemical  $CO_2RR$ . [11]

In comparison with A-CuNWs, H-CuNWs with a thicker oxide sheath and smoother surface showed a slightly lower FE toward ethylene: 52.0 % at  $-1.02~V_{RHE}$  (Figure 3b). The total yield for C<sub>2+</sub> products reached 71.9 % while the proportion of H<sub>2</sub> was at 11.4%, together with low yields for both CO and  $\mathrm{CH_4}$  (2.0 and 6.1 %, respectively). At  $-1.02~\mathrm{V_{RHE}}$ , a geometric current density of 24.1 mA cm<sup>-2</sup> was achieved for all the products, with a partial current density of 12.5 mA cm<sup>-2</sup> for ethylene (Figure 3 c,d). Although slightly lower than A-CuNWs, a mass activity approaching 246.2 mA mg<sup>-1</sup> was obtained for ethylene production when H-CuNWs served as the catalyst (Figure S4). When normalized to the electrochemically active surface area (ECSA), we obtained partial current densities as high as 4.1 and 3.5 mA cm<sup>-2</sup> toward ethylene for A-CuNWs and H-CuNWs, respectively, demonstrating their outstanding performance in CO<sub>2</sub>RR (Figure S5 and S6, the current densities of comparable catalysts can be found in Table S1). It should be noted that the high (approaching 30 mA cm<sup>-2</sup>) geometric current densities achieved by CuNWs could be attributed to the involvement of 3D mass transport, which raised the limitation of current density.[24]

To look into the mechanism underlying the high selectivity and activity of CuNW-based catalysts and the reason why they behaved differently, we characterized the structures of both catalysts after 1 h of electrolysis at  $-1.02\,\mathrm{V}_\mathrm{RHE}$ . As shown in Figure 4a, fragmentation was observed for A-CuNWs, where small pseudo-spherical nanoparticles and nanorods resulted from disintegration of nanowires could be found in the TEM image. For the nanowires whose 1D structure was preserved, their surface became fairly rough. A close examination of the nanowire illustrated the existence of large holes and cavities on the surface, which could be attributed to the reduction of surface oxides (Figure 4b). As shown by the bright-field STEM (BF-STEM) image in Figure 4c, the lattice spacing of 0.21 and 0.18 nm could be assigned to the {111} and {200} planes of Cu, respectively,

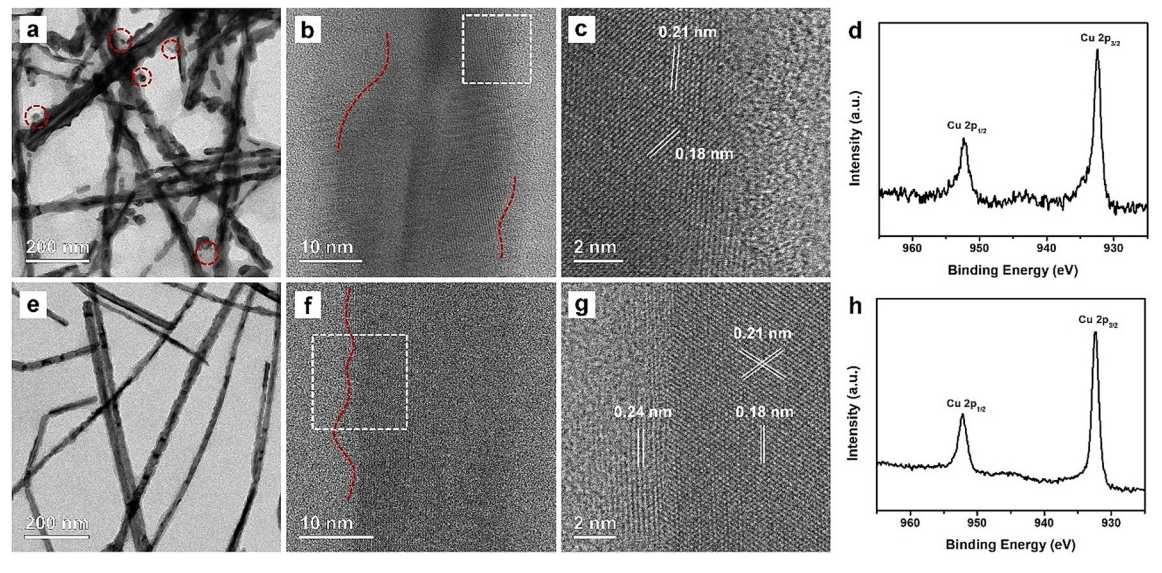


Figure 4. a) TEM, b,c) BF-STEM images, and d) XPS spectrum of A-CuNWs after 1 h of electrolysis. e) TEM, f,g) BF-STEM images, and h) XPS spectrum of H-CuNWs after 1 h of electrolysis. A potential of  $-1.02\,V_{RHE}$  was applied for all measurements. The images in (c) and (g) were taken from the regions marked by boxes in (b) and (f), respectively. The Cu nanoparticles formed during electrolysis are marked by red circles in (a).





confirming that the majority of surface Cu<sub>x</sub>O was reduced to metallic Cu. The conversion of oxide sheath was also revealed by XPS. Compared to the relatively strong peaks of copper oxides in the as-prepared A-CuNWs (Figure 1e), no satellite peaks were observed for the same sample after 1 h of electrolysis (Figure 4d), confirming the reduction of Cu<sup>II</sup> to Cu<sup>0</sup> or Cu<sup>I</sup>. Considering the larger lattice spacing of copper oxides and possible surface reconstruction, voids would be generated for the formation of cavities on the surface when Cu<sub>r</sub>O was reduced to metallic Cu.<sup>[25]</sup> The non-uniform thickness of oxide layer caused by the slow oxidation kinetics of O<sub>2</sub> from air resulted in the formation of voids with different sizes and thus the presence of deep cavities, increasing the chance of breaking up the nanowires. In addition to the reduction of copper oxides, detachment of small nanoparticles from the CuNWs during electrolysis might also facilitate their fragmentation.<sup>[26]</sup> It was reported that the adsorption of either H or CO, intermediates in HER and CO2RR, on the surface of Cu nanocubes would lead to degradation to the shapes when a low potential was applied. An increased number of pinholes on the surface and a decrease in the size of Cu nanocubes were observed, along with an increased number of nanoparticles emerging around the cubes.<sup>[27]</sup> This was similar to what we observed on A-CuNWs.

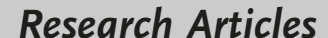
In contrast to the A-CuNWs, the 1D morphology of the H-CuNWs was largely retained during electrolysis. As shown in Figure 4e, we found nearly no fragment around the nanowires, let alone their disintegration. Compared with the smooth surface of H-CuNWs before electrolysis, the surface roughness was increased after being held at  $-1.02 V_{RHE}$  for 1 h (Figure 2a). As shown by the BF-STEM image in Figure 4 f, small, shallow voids were formed on the surface. The magnified, atomic-resolution image revealed the presence of metallic Cu on the surface, where the lattice spacing of 0.21 and 0.18 nm could be indexed to the Cu {111} and {100} planes (Figure 4g). Some copper oxides were also observed outside the metallic Cu core, but they were highly possible to be generated during the preparation of sample for STEM imaging. Similar to the A-CuNWs, the XPS peaks of CuO disappeared after electrolysis, confirming the reduction of Cu<sup>II</sup> to Cu<sup>0</sup> or Cu<sup>I</sup> (Figure 4h). To further verify the oxidation state of Cu on the surface, we measured the Auger Cu LMM spectra of the nanowires before and after electrolysis (Figure S7). The samples were protected by Ar throughout the transfer process. Before electrolysis, the surface oxides of both types of nanowires were mainly composed of CuO, as revealed by the peaks located at 568.9 eV. After 1 h of electrolysis, we observed both Cu<sup>0</sup> and Cu<sup>1</sup> peaks located at 568.0 and 569.8 eV, respectively, suggesting the presence of Cu<sup>I</sup> ions in the catalysts. It is worth pointing out that the retention of Cu<sup>I</sup> species during electrolysis was also observed in recent studies involving both ex situ and in situ techniques.[10,12,13,27-29]

Based on TEM and STEM imaging, the high yields of  $C_{2+}$  products for CuNWs covered with an oxide sheath can be mainly attributed to their increased surface roughness.<sup>[5,25,30,31]</sup> As previously reported, roughening the surface of Cu catalysts would lead to the generation of a greater density of defective sites, which can enhance the adsorption of  $C_1$ 

intermediates and thus improve the catalyst's selectivity toward C<sub>2+</sub> products.<sup>[30]</sup> In addition to surface roughness, several other factors, including the presence of twin defects and 1D morphology of the nanowires, may also be involved. [6,32] Based on simulations from previous reports, the twin boundaries and tensile surface strain, together with stacking faults arising from a stress release mechanism, could enhance the adsorption of CO on Cu surface and increase CO coverage density, which in turn facilitated the C-C coupling and formation of C<sub>2+</sub> products.<sup>[6]</sup> As such, the high yields of C<sub>2+</sub> species may also benefit from the penta-twinned structure of the CuNWs. Moreover, the small diameter of the nanowires and their 1D morphology also enlarged the specific surface area and improved the mass transport in electrocatalysis, contributing to a high mass activity. [33,34] As a comparison, when H<sub>2</sub>O<sub>2</sub>-oxidized Cu nanoparticles were used as the catalyst, a FE of 41.8% toward ethylene was obtained at  $-1.05 V_{RHE}$ , together with a geometric partial current density of 6.8 mA cm<sup>-2</sup> (Figure S8). The inferior selectivity and lower current density of the nanoparticles further demonstrate the importance of both the 1D morphology and twinned structure of the nanowires in improving mass transport and facilitating C-C coupling.<sup>[34]</sup>

Comparing the shape evolution of two types of CuNWs during  $CO_2RR$ , we proposed that the higher  $C_{2+}$  selectivity of A-CuNWs relative to that of H-CuNWs could be ascribed to their even greater surface roughness. As confirmed by the TEM and STEM images in Figure 4b,f, deeper cavities were observed on A-CuNWs, and they were reported to help trap the C<sub>1</sub> and even C<sub>2</sub> intermediates and thus facilitate C-C coupling. [35,36] Besides, the greater extent of roughness also revealed the potential existence of a higher abundance of high-index facets and defective sites on the surface of A-CuNWs, which had been proven to promote the formation of C<sub>2+</sub> products.<sup>[7,25]</sup> In addition to selectivity, the greater surface roughness also contributed to a larger specific surface area and thus higher mass activity of A-CuNWs compared to H-CuNWs. As shown in Figure S5 and Table S2, double-layer capacitances of different types of nanowires were measured, correlating their activities with surface areas. A capacitance of 140 μF cm<sup>-2</sup> was obtained for A-CuNWs, which was 40% greater than that of H-CuNWs, consistent with the higher mass activity of A-CuNWs. When using pristine CuNWs as a reference, both A-CuNWs and H-CuNWs exhibited larger capacitances (with a factor of 3.0 and 2.2, respectively), revealing their increase in surface roughness arising from the presence and subsequent reduction of surface oxides. We also tried to measure the CO<sub>2</sub>RR performance of pristine CuNWs as soon as they were prepared, with an effort to avoid significant oxidation like in the case of A-CuNWs. Compared with the surface-oxidized nanowires, pristine CuNWs showed a relatively lower  $C_{2+}$  selectivity (66.0%) at  $-1.07\,V_{RHE}$ owing to the absence of extensive surface oxidation and thus the lower surface roughness (Figure S9).

The stability of the CuNW-based catalysts was then measured at  $-1.02\,\mathrm{V_{RHE}}$ , corresponding to the highest ethylene selectivity. For A-CuNWs, the FE of ethylene gradually decreased as the reaction time was extended, along with an increase in the yields of  $\mathrm{H_2}$  and  $\mathrm{CH_4}$  (Figure 5a),







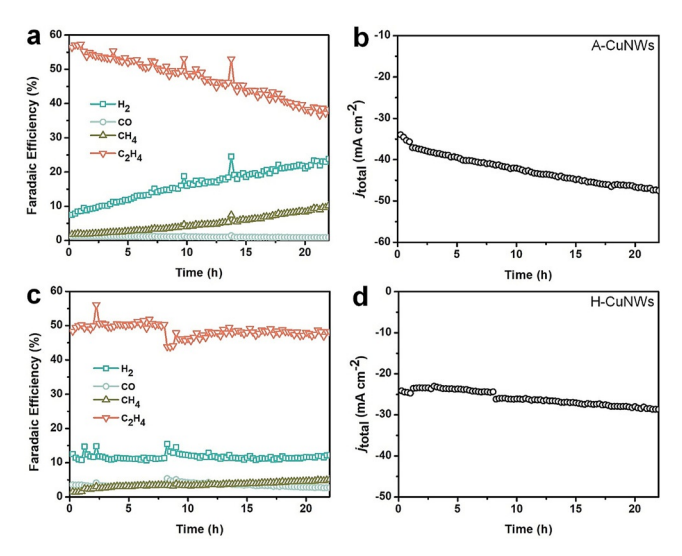


**Figure 5.** Stability tests for the catalysts based on a,b) A-CuNWs and c,d) H-CuNWs, respectively, at  $-1.02\,V_{RHE}$  for 22 h: Faradaic efficiencies of gaseous products (a,c) and current densities normalized to the geometric area (b,d).

which could be mainly attributed to the severe fragmentation of A-CuNWs during the measurement. It has been suggested by many reports that the selectivity of Cu catalysts is highly related to the particle size. [37,38] When the particle size of Cu decreased, below 5 nm in particular, a dramatic increase in activity and selectivity toward HER was observed, which can be ascribed to the increased proportion of atoms located at edges and corners. Those atoms have relatively low coordination numbers and can serve as strong binding sites for H and CO, limiting their diffusion on surface and further reaction to generate C<sub>2+</sub> products. Under this circumstance, HER was greatly facilitated due to the improved adsorption of protons on Cu surface while the production of C<sub>2+</sub> species was suppressed.<sup>[38]</sup> Along with the decrease in selectivity toward ethylene, an increase in the total current density by about 40% was also observed after 22 h (Figure 5b), confirming the fragmentation of A-CuNWs and further enlargement in specific surface area.

When H-CuNWs served as the catalyst, the selectivity toward ethylene showed nearly no decay after 22 h, indicating its superb stability (Figure 5c). In the meantime, the current density of H-CuNWs also stayed relatively constant during the measurement, with an increase less than 5 mA cm<sup>-2</sup> (or 20%) (Figure 5d). To understand the enhanced stability, TEM imaging was conducted on both types of CuNWs after 5 h of electrolysis and the results are shown in Figure S10. In the case of A-CuNWs, broken nanowires and Cu nanoparticles, either separated from or attached to the nanowires, were observed (Figure S10a-c). As for H-CuNWs, very few of them were fragmented (Figure S10d-f). Regarding the difference in morphology, we proposed that the different oxidation pathways and the resultant structures of oxide layers were responsible for the difference in stability. The non-uniform oxidation and the resultant deep cavities led to easier disintegration of nanowires, as mentioned previously, resulting in the poor stability of A-CuNWs. In contrast, for H-

CuNWs covered by a thicker and smoother Cu<sub>r</sub>O layer, the metallic Cu core was well protected during the CO<sub>2</sub>RR. Though the surface oxides were reduced during catalysis, no large voids were developed on surface and the continuity of the nanowires was well preserved. The preservation of 1D morphology and suppression of fragmentation by introducing a thick, smooth oxide sheath contributed to an improved stability for H-CuNWs.[39] However, it should be pointed out that although higher durability was achieved for H-CuNWs, they suffered slightly in terms of selectivity and activity when compared to A-CuNWs. Besides, the increase in current density as a function of time also revealed that the fragmentation could be effectively retarded for H-CuNWs, but not completely eliminated. At the moment, it remains a major challenge to design catalysts with both good stability and high selectivity and activity. Addition of supports to stabilize catalysts or covering the surface of a catalyst with proper ligands to prevent surface reconstruction might be promising directions in further research.[40]

#### Conclusion

In summary, we have demonstrated two effective CO<sub>2</sub>RR catalysts based on CuNWs with their surface being partially oxidized through different pathways. The A-CuNWs obtained via oxidation by the O<sub>2</sub> from air possessed a rough surface and a thin oxide layer with non-uniform thickness, while the H-CuNWs obtained by oxidation with aqueous H<sub>2</sub>O<sub>2</sub> were covered with a relatively thicker and smoother oxide sheath. When applied to electrochemical CO<sub>2</sub>RR, both of them exhibited high selectivity and activity toward C<sub>2+</sub> species, ethylene in particular. The greater extent of surface roughness, the presence of more defective sites and deeper cavities after reduction of non-uniform oxide sheath contributed to a higher C<sub>2+</sub> selectivity for A-CuNWs relative to H-CuNWs. However, these features were also detrimental to the stability of A-CuNWs due to their increased susceptibility to disintegration during electrolysis. Protected by a thicker and smoother Cu<sub>x</sub>O layer, the fragmentation of nanowires was effectively suppressed for H-CuNWs and nearly no decay in ethylene selectivity was observed after 22 h, demonstrating the improved catalytic stability. Taken together, this work demonstrates that controlling surface oxidation offers an effective strategy for improving both the C2+ selectivity and stability of Cu-based catalysts. We believe the same strategy should be extendible to other types of Cu nanostructures for the rational development of effective catalysts toward  $CO_2RR$ .

## Acknowledgements

This work was supported in part by a grant from the NSF (CHE 1804970), start-up funds from the Georgia Institute of Technology, two grants from the Research Grant Council of Hong Kong SAR (26206115 and 16309418), and one from Hong Kong Branch of Southern Marine Science and Engineering Guangdong Laboratory (SMSEGL20SC01). TEM



# Research Articles



and STEM imaging were performed at the Materials Characterization Facilities of the GT's Institute of Electronics and Nanotechnology (IEN), a member of the National Nanotechnology Coordinated Infrastructure (NNCI) and supported by the National Science Foundation (ECCS-1542174). Part of the STEM imaging and EELS mapping in this research were completed at the Center for Nanophase Materials Sciences, which is a DOE Office of Science User Facility. S. Zhu thanks the financial support from Research Grant Council Postdoctoral Fellowship Scheme (PDFS2021-6S08). We thank Prof. Mingjie Zhang and Mr. Rui Feng from HKUST for providing the NMR facility.

### Conflict of interest

The authors declare no conflict of interest.

**Keywords:**  $C_{2+}$  selectivity  $\cdot$  copper nanowires  $\cdot$  electrochemical  $CO_2$  reduction  $\cdot$  nanocatalysis  $\cdot$  surface oxidation

- [1] D. Gao, R. M. Arán-Ais, H. S. Jeon, B. Roldan Cuenya, *Nat. Catal.* 2019, 2, 198–210.
- [2] S. Nitopi, E. Bertheussen, S. B. Scott, X. Liu, A. K. Engstfeld, S. Horch, B. Seger, I. E. L. Stephens, K. Chan, C. Hahn, J. K. Nørskov, T. F. Jaramillo, I. Chorkendorff, *Chem. Rev.* 2019, 119, 7610–7672.
- [3] R. M. Arán-Ais, D. Gao, B. Roldan Cuenya, Acc. Chem. Res. 2018, 51, 2906–2917.
- [4] Y. Hori, I. Takahashi, O. Koga, N. Hoshi, J. Mol. Catal. A Chem. 2003, 199, 39 – 47.
- [5] C. Reller, R. Krause, E. Volkova, B. Schmid, S. Neubauer, A. Rucki, M. Schuster, G. Schmid, Adv. Energy Mater. 2017, 7, 1602114.
- [6] C. Choi, T. Cheng, M. Flores Espinosa, H. Fei, X. Duan, W. A. Goddard, Y. Huang, Adv. Mater. 2019, 31, 1805405.
- [7] H. S. Jeon, S. Kunze, F. Scholten, B. Roldan Cuenya, ACS Catal. 2018, 8, 531 – 535.
- [8] D. Kim, J. Resasco, Y. Yu, A. M. Asiri, P. Yang, Nat. Commun. 2014, 5, 4948.
- [9] Z. Q. Liang, T. T. Zhuang, A. Seifitokaldani, J. Li, C. W. Huang, C. S. Tan, Y. Li, P. De Luna, C. T. Dinh, Y. Hu, Q. Xiao, P. L. Hsieh, Y. Wang, F. Li, R. Quintero-Bermudez, Y. Zhou, P. Chen, Y. Pang, S. C. Lo, L. J. Chen, H. Tan, Z. Xu, S. Zhao, D. Sinton, E. H. Sargent, Nat. Commun. 2018, 9, 3828.
- [10] Y. Zhou, F. Che, M. Liu, C. Zou, Z. Liang, P. De Luna, H. Yuan, J. Li, Z. Wang, H. Xie, H. Li, P. Chen, E. Bladt, R. Quintero-Bermudez, T. K. Sham, S. Bals, J. Hofkens, D. Sinton, G. Chen, E. H. Sargent, *Nat. Chem.* 2018, 10, 974–980.
- [11] H. Jung, S. Y. Lee, C. W. Lee, M. K. Cho, D. H. Won, C. Kim, H. S. Oh, B. K. Min, Y. J. Hwang, J. Am. Chem. Soc. 2019, 141, 4624–4633.
- [12] J. Kim, W. Choi, J. W. Park, C. Kim, M. Kim, H. Song, J. Am. Chem. Soc. 2019, 141, 6986–6994.
- [13] D. Gao, I. Zegkinoglou, N. J. Divins, F. Scholten, I. Sinev, P. Grosse, B. Roldan Cuenya, ACS Nano 2017, 11, 4825–4831.
- [14] M. Luo, M. Zhou, R. R. Da Silva, J. Tao, L. Figueroa-Cosme, K. D. Gilroy, H. C. Peng, Z. He, Y. Xia, *ChemNanoMat* **2017**, *3*, 190–195.
- [15] J. C. Yang, B. Kolasa, J. M. Gibson, M. Yeadon, Appl. Phys. Lett. 1998, 73, 2841 – 2843.

- [16] J. A. Eastman, P. H. Fuoss, L. E. Rehn, P. M. Baldo, G. W. Zhou, D. D. Fong, L. J. Thompson, *Appl. Phys. Lett.* **2005**, 87, 051914.
- [17] Z. Lyu, M. Xie, E. Aldama, M. Zhao, J. Qiu, S. Zhou, Y. Xia, ACS Appl. Nano Mater. 2019, 2, 1533–1540.
- [18] H. Han, H. Choi, S. Mhin, Y.-R. Hong, K. M. Kim, J. Kwon, G. Ali, K. Y. Chung, M. Je, H. N. Umh, D. H. Lim, K. Davey, S. Z. Qiao, U. Paik, T. Song, *Energy Environ. Sci.* **2019**, *12*, 2443–2454.
- [19] D. DeNardis, D. Rosales-Yeomans, L. Borucki, A. Philipossian, Thin Solid Films 2006, 513, 311–318.
- [20] M. Yin, C. K. Wu, Y. Lou, C. Burda, J. T. Koberstein, Y. Zhu, S. O'Brien, J. Am. Chem. Soc. 2005, 127, 9506-9511.
- [21] Z. Lyu, M. Xie, K. D. Gilroy, Z. D. Hood, M. Zhao, S. Zhou, J. Liu, Y. Xia, Chem. Mater. 2018, 30, 6469 – 6477.
- [22] H. Guo, N. Lin, Y. Chen, Z. Wang, Q. Xie, T. Zheng, N. Gao, S. Li, J. Kang, D. Cai, D. L. Peng, Sci. Rep. 2013, 3, 2323.
- [23] L. L. Hung, C. K. Tsung, W. Huang, P. Yang, Adv. Mater. 2010, 22, 1910–1914.
- [24] D. Raciti, M. Mao, C. Wang, Nanotechnology 2018, 29, 044001.
- [25] A. D. Handoko, C. W. Ong, Y. Huang, Z. G. Lee, L. Lin, G. B. Panetti, B. S. Yeo, J. Phys. Chem. C 2016, 120, 20058–20067.
- [26] J. Huang, N. Hörmann, E. Oveisi, A. Loiudice, G. L. De Gregorio, O. Andreussi, N. Marzari, R. Buonsanti, *Nat. Commun.* 2018, 9, 2551.
- [27] H. Mistry, A. S. Varela, C. S. Bonifacio, I. Zegkinoglou, I. Sinev, Y. W. Choi, K. Kisslinger, E. A. Stach, J. C. Yang, P. Strasser, B. Roldan Cuenya, *Nat. Commun.* 2016, 7, 12123.
- [28] F. Cavalca, R. Ferragut, S. Aghion, A. Eilert, O. Diaz-Morales, C. Liu, A. L. Koh, T. W. Hansen, L. G. M. Pettersson, A. Nilsson, J. Phys. Chem. C 2017, 121, 25003 – 25009.
- [29] Y. Zhao, X. Chang, A. S. Malkani, X. Yang, L. Thompson, F. Jiao, B. Xu, J. Am. Chem. Soc. 2020, 142, 9735 9743.
- [30] W. Tang, A. A. Peterson, A. S. Varela, Z. P. Jovanov, L. Bech, W. J. Durand, S. Dahl, J. K. Nørskov, I. Chorkendorff, *Phys. Chem. Chem. Phys.* 2012, 14, 76–81.
- [31] X. Feng, K. Jiang, S. Fan, M. W. Kanan, ACS Cent. Sci. 2016, 2, 169–174.
- [32] H. Zhang, Y. Zhang, Y. Li, S. Ahn, G. T. R. Palmore, J. Fu, A. A. Peterson, S. Sun, *Nanoscale* 2019, 11, 12075 – 12079.
- [33] Z. Chen, M. Waje, W. Li, Y. Yan, Angew. Chem. Int. Ed. 2007, 46, 4060–4063; Angew. Chem. 2007, 119, 4138–4141.
- [34] D. Huo, M. J. Kim, Z. Lyu, Y. Shi, B. J. Wiley, Y. Xia, Chem. Rev. 2019, 119, 8972–9073.
- [35] T. T. Zhuang, Y. J. Pang, Z. Q. Liang, Z. Y. Wang, Y. Li, C. S. Tan, J. Li, C. T. Dinh, P. De Luna, P. L. Hsieh, T. Burdyny, H. H. Li, M. X. Liu, Y. H. Wang, F. W. Li, A. Proppe, A. Johnston, D. H. Nam, Z. Y. Wu, Y. R. Zheng, A. H. Ip, H. R. Tan, L. J. Chen, S. H. Yu, S. O. Kelley, D. Sinton, E. H. Sargent, *Nat. Catal.* 2018, 1, 946–951.
- [36] K. D. Yang, W. R. Ko, J. H. Lee, S. J. Kim, H. Lee, M. H. Lee, K. T. Nam, Angew. Chem. Int. Ed. 2017, 56, 796–800; Angew. Chem. 2017, 129, 814–818.
- [37] A. Loiudice, P. Lobaccaro, E. A. Kamali, T. Thao, B. H. Huang, J. W. Ager, R. Buonsanti, *Angew. Chem. Int. Ed.* 2016, 55, 5789 – 5792; *Angew. Chem.* 2016, 128, 5883 – 5886.
- [38] R. Reske, H. Mistry, F. Behafarid, B. Roldan Cuenya, P. Strasser, J. Am. Chem. Soc. 2014, 136, 6978-6986.
- [39] C. W. Li, M. W. Kanan, J. Am. Chem. Soc. 2012, 134, 7231 7234.
- [40] J. Fu, W. Zhu, Y. Chen, Z. Yin, Y. Li, J. Liu, H. Zhang, J. J. Zhu, S. Sun, Angew. Chem. Int. Ed. 2019, 58, 14100–14103; Angew. Chem. 2019, 131, 14238–14241.

Manuscript received: September 1, 2020 Accepted manuscript online: October 2, 2020 Version of record online: November 20, 2020